Geophysical Research Letters

RESEARCH LETTER
10.1029/2020GL091462

Intensified Humid Heat Events Under Global Warming

Pinya Wang[1], Yang Yang[1], Jianping Tang[2], L. Ruby Leung[3], and Hong Liao[1]

[1]Jiangsu Key Laboratory of Atmospheric Environment Monitoring and Pollution Control, Jiangsu Collaborative Innovation Center of Atmospheric Environment and Equipment Technology, School of Environmental Science and Engineering, Nanjing University of Information Science and Technology, Nanjing, Jiangsu, China, [2]School of Atmospheric Sciences, Nanjing University, Nanjing, Jiangsu, China, [3]Atmospheric Sciences and Global Change Division, Pacific Northwest National Laboratory, Richland, WA, USA

Abstract Based on the Coupled Model Intercomparison Project Phase 5 multimodel simulations, this paper investigates the future changes in extreme wet-bulb temperatures (TWs) and extreme dry-bulb temperatures (Ts) globally under both low-emission and high-emission scenarios (Representative Concentration Pathways of 4.5 [RCP4.5] and 8.5 [RCP8.5]). Under a warming climate, T and TW exhibit a higher absolute increase in their mean values over the mid–high latitudes while they show higher relative increases in their mean values and variability over tropics. Humid and dry heat events which consist of consecutive extreme TWs and Ts show higher occurrences over tropics, governed by the joint increases in mean values and variability of TW and T therein. Humid heat events show intensifications to dry heat events with higher frequency, duration, and intensity, driven by the lower variability of TW than T. In the mid–high latitudes, heat events will start earlier and last longer in warm season under RCP8.5 than RCP4.5, motivating the need for global warming mitigation.

Plain Language Summary The adverse impacts of high temperatures and high humidity on health and economics are worse than extreme temperatures alone. Wet-bulb temperature (TW) combining temperature (T) and humidity is a useful index for humid heat. We investigate future changes in extreme TWs and Ts based on a set of simulations under low-emission and high-emission scenarios. In a warmer climate, both extreme TWs and Ts show apparent absolute increases over the mid–high latitudes but higher increases in mean values and variability in relative terms over tropics. Governed by the joint impacts of mean values and variability of TWs and Ts, humid and dry heat events featuring consecutive days of extreme TWs and Ts show higher occurrences in the tropics. Future humid heat events are more frequent, intense, and longer lasting than dry heat events as TW is more sensitive to global warming than T. Both humid and dry heat events start earlier and last longer under the high-emission than low-emission scenario.

Key Points:

- Extreme high wet-bulb temperature is more sensitive to the changing climate than extreme high dry-bulb temperature
- Future heat events have relatively higher occurrences in the tropics, and humid heat events are substantially intensified than dry heat
- The intensification of humid heat events is associated with the projected increases in specific humidity in the warmer climate

Supporting Information:

- Supporting Information S1

Correspondence to:
Y. Yang and J. Tang,
yang.yang@nuist.edu.cn;
jptang@nju.edu.cn

Citation:
Wang, P., Yang, Y., Tang, J., Leung, L. R., & Liao, H. (2021). Intensified humid heat events under global warming. *Geophysical Research Letters*, *48*, e2020GL091462. https://doi.org/10.1029/2020GL091462

Received 2 NOV 2020
Accepted 5 DEC 2020

1. Introduction

Global warming has been detected during the twentieth century and enhanced since the late 1970s (Trenberth et al., 2007). The globally averaged surface air temperature has increased by more than 1°C since 1880. (Lenssen et al., 2019) and is expected to rise by 1.4–5.8°C from 1990 to 2100 (Boo et al., 2006). Under global warming, extreme heat events have been a great public concern because of their socioeconomic impacts (Mukherjee et al., 2020). For example, the extreme 2003 heat wave in Europe (Black et al. 2004; Stéfanon et al. 2012), the hot summer of 2010 in Russia (Dole et al., 2011; Matsueda, 2011), and the extreme 2013 heat wave in China (Xia et al., 2016) have caused billions of economic losses and abruptly increased heat-related morbidity and mortality. Great efforts have been made to understand the future projections of heat events at global and regional scales (e.g., Boo et al., 2006; Kunkel et al., 2010). Beniston et al. (2007) found the regional surface warming over Europe would cause the frequency, intensity, and duration of heat waves to increase therein. Dosio et al. (2018) demonstrated that heat waves are expected to be more severe over Africa, South America, and Southeast Asia under a warmer climate.

Most current works focus on extreme dry-bulb temperatures while heat-related mortality rates are sharply enhanced under both high temperature and humidity (Conti et al., 2005; Willet & Sherwood, 2012). Humid and warm conditions can restrain the sweating efficiency of the human body. Accumulation of environmental and metabolic heat in the body would eventually cause physical disorders and even deaths

(Budd, 2008; Davis et al., 2016; Hanna & Tait, 2015; Mora et al., 2017). Hence, understanding the future projections of humid heat stress involving both humidity and dry-bulb temperatures is of great significance for understanding human and ecosystem acclimation in future climate and for policymakers to advance climate change adaptations (e.g., Caulfield et al., 2014; Pielke et al., 1998; Zhai et al., 2018).

Among several integral heat indices that consider both humidity and dry-bulb temperature conditions, wet-bulb temperature (TW) is an effective measure for characterizing extreme humid heat stress. TW is the temperature of adiabatic saturation. TW is lower than the dry-bulb temperatures but will be identical with 100% relative humidity. Other integrated heat indices including the wet-bulb globe temperature (WBGT) have also been used in recent studies (Fischer & Knutti, 2013). There are two types of WBGT, the indoor WBGT and the outdoor WBGT. The indoor WBGT involves the effects of dry-bulb temperature and humidity and the outdoor WBGT additionally incorporates the effects of sunlight and wind (Li et al., 2017). WBGT is more often used in health-related studies because there are established safety thresholds for WGBT (Willet & Sherwood, 2012). However, this variable is difficult to measure. In contrast, TW can be accurately measured based on thermodynamic principle (Sherwood & Huber, 2010) so it has been widely used in climate studies (e.g., Kang & Eltahir, 2018; Raymond et al., 2017; 2020). Most of them focus on individual days of high TWs. However, the impacts of temperature extremes on human health relate not only to individual hot days but are strongly affected by the persistence and intensity of temperature extremes.

Here, using 18 global climate models (GCMs) from Coupled Model Intercomparison Project Phase 5 (CMIP5, Taylor et al., 2012), we project the future changes of extreme TWs on a global scale under two Representative Concentration Pathways of 4.5 (RCP4.5) and 8.5 (RCP8.5), respectively, and compare results between the low-emission and high-emission scenarios. Future projections of the frequency, duration, and intensity of extreme heat events consisting of several consecutive days of extreme TWs are also examined.

2. Data and Methods

2.1. Data

The calculation of daily maximum wet-bulb temperature (hereafter, referred to as TW) is based on the dry-bulb temperature (T, in this case daily maximum air temperature), daily mean specific humidity, and surface pressure using the algorithm described in Davies-Jones (2008), implemented in HumanIndexMod by Buzan et al (2015), and ported to Matlab by Dr Robert Kopp. The daily data sets are the outputs of historical (Hist, 1981–2005) and future (Fut, 2076–2100) simulations by 18 GCMs from CMIP5 forced by the RCP4.5 and RCP8.5 scenarios, respectively (Table S1). The number of models chosen is solely based on data availability.

Daily data from NCEP Reanalysis II (NCEP2, Kanamitsu et al., 2002) and ECMWF Re-Analysis Interim (ERA-Interim, Dee et al., 2011) are used to validate the historical simulation from 1980 to 2005. The two reanalysis data sets are widely used to validate extreme temperatures in CMIP5 simulations (e.g., Dosio et al., 2018; Koutroulis et al., 2016; Kumar et al., 2014). The reanalysis and GCM data are regridded to 2° × 2° resolution using linear interpolation to facilitate spatial comparison. The multimodel ensemble mean (MME) can effectively suppress internal variability and isolate the effects of global warming as internal variability is not synchronous across the individual simulations in the CMIP5 ensemble (Dong et al., 2018; Zhao et al., 2014). The MME is calculated as the arithmetic mean of the equally weighted 18 CMIP5 models, supposing all the models involved are independent though many climate models tend to be correlated (Huang et al., 2019)

2.2. Identifications of Extreme Heat Events

We identify extreme heat events based on both daily maximum TW and T at each grid point during 2076–2100 under RCP4.5 and RCP8.5, respectively. Specifically, humid and dry heat events, referred to as HE_TW and HE_T, consist of at least three consecutive days of extremely high TWs and Ts above the historical mean annual maximum wet-bulb temperatures (TWx) and dry-bulb temperature (Tx), respectively. HE_TW and HE_T are characterized by the number (HN), duration (HDU), intensity (HI), and sum of participating days

(HF) of heat events. At each grid point over a specific period (e.g., 1 year or the whole analysis period), HN is the total number of heat event occurrences (unit: events), HDU is the average duration (unit: days/event), HI is the average intensity (unit: event^{-1}), and HF is the total days of heat events (unit: days). These heat indices are suffixed by "TW" or "T" (e.g., HN_TW and HN_T) and defined following Wang et al. (2019):

$$\mathrm{HN} = N \tag{1}$$

$$\mathrm{HDU} = \sum_{i=1}^{N}(D_i) \Big/ N \tag{2}$$

$$\mathrm{HF} = \sum_{i}^{N} D_i = \mathrm{HDU} \times \mathrm{HN} \tag{3}$$

$$\mathrm{HI} = \sum_{i}^{N}\sum_{j}^{D_i}\left(\mathrm{T}_{ij} - \mathrm{Ta}\right) / \mathrm{IQR} \Big/ N \tag{4}$$

where N is the total number of heat events during the period; for a specific heat event i based on TW or T, its intensity $\sum_{j}^{Di}\left(\mathrm{T}_{ij} - \mathrm{Ta}_{ij}\right) / \mathrm{IQR}$ is calculated as the sum of the temperature deviation normalized by the local historical interquartile range (IQR). The IQR of TWx or Tx is defined as the difference between the 75th and 25th percentile of yearly TWx or Tx during 1981–2005. T_{ij} is daily maximum TW or T for day j within the duration D_i of the event. Ta is the mean TWx or Tx for 1981–2005. Hence, both the occurrence and the intensity of heat events in future are defined with respect to the historical climate. Note that HI is an integral index that considers both the temperature anomalies and the duration of heat events. HI uses the historical IQR value of annual TWx or Tx to normalize the magnitude of heat events. A heat event with HI_TW or HI_T equals to n indicates that its intensity is n times the climatological IQR. Note that HF is also an integral index that combines the characteristics of HN and HDU.

2.3. Model Representation of Extreme TWs and Ts Under Historical Climate

The CMIP5 model performance in simulating the historical yearly TWx and Tx is evaluated by comparing the simulations with the reanalysis. Regional analysis is performed for 21 subregions (Figure 1(a)) as defined in Giorgi and Francisco (2000). The historical (1981–2005) mean TWx in the MME (Figure S1(a)) shows similar spatial pattern with those in ERA-Interim and NCEP2 reanalysis (Figures S1(b) and S1(c)), with higher values over the tropics and midlatitudes (except the high-latitude Tibetan Plateau region) relative to the high latitudes. The spatial correlation coefficient between the historical mean TWx in the MME and the mean TWx in ERA-Interim (NCEP2) reanalysis data is 0.68 (0.70), exceeding the 95% confidence level. The good model performance in simulating extreme TWs is further supported by the regional mean results (Figure S1(d)), with the bias between the MME and ERA-Interim (NCEP) within −1.0°C to 0.5°C (−1.1°C to 0.4°C) over all subregions. And the intermodel spread is much lower compared to the ensemble mean values over all the subregions (Figure S1(d)), suggesting the low uncertainties across the multimodel simulations. The small intermodal spread among the 18 GCMs in simulating the spatial features of TWx is further confirmed by Figure S1(e), and the MME performs better than most of the single ones. In addition, the MME shows a good spatial representation for Tx (Figure S2). Moreover, the historical mean TWx and Tx in model results over subtropics and midlatitudes are supported by the HadISD observation data set (Figure S3), which is produced by the Met Office Hadley Centers as a rigorously quality control versioned of the National Climatic Data Center Integrated Surface Database (Dunn et al., 2012, 2016).

The historical IQR values of yearly TWx and Tx represent the interannual variability of extreme TWs and Ts, respectively. Contrary to the spatial pattern of mean values of extreme TWx and Tx, the interannual variability of both the annual TWx and Tx is higher over the mid–high latitudes with higher synoptic variability but lower over the tropical regions (Figures S4(a) and S4(d)). Moreover, Tx generally shows higher variability than TW across the globe under historical climate. Furthermore, the MME satisfactorily reproduces the spatial patterns of IQR values of TWx and Tx of the reanalysis (Figures S4(b) and S4(c) and S4(e) and S4(f)), with significant spatial correlation coefficients above 0.45.

3. Results

3.1. Future Changes in Extreme TW and T

Figure 1 illustrates the spatial distributions of future changes in extreme TWs and Ts projected by the MME of 18 CMIP5 models under the RCP8.5 scenario by comparing the average yearly TWx and Tx between 2076–2100 and 1981–2005. The robustness of the multimodel projections is shown in Figure S5. For a comprehensive view of the future changes, both the absolute changes in the average TWx and Tx between the historical and the future periods (Fut–Hist) and the relative changes of TWx and Tx, defined as the absolute changes normalized by the historical IQR values, are examined. Since the relative changes of TWx and Tx account for both the historical variability and the absolute future changes, it is more representative of the sensitivity of TW and T to climate change (Wang et al., 2019). The average TWx in the MME shows robust increases globally under RCP8.5, with larger increases around 3–4°C over the mid–high latitudes while changes are smaller in the tropical regions (Figure 1(a)). However, the relative changes of extreme TWs show higher magnitudes in the tropical regions between 30°S and 30°N (Figure 1(b)), especially over Southeast Asia (SEA subregion), which is partly due to the lower interannual variability of TWs in the tropics (Figure S4). Although both the absolute changes of TWx and Tx show apparent increases globally (Figure 1(a) and 1(c)), the absolute changes of Tx show greater magnitude over the mid–high latitudes except the Greenland while the absolute changes of TWx show higher increases over the North Hemisphere than the South Hemisphere, which may be due to the higher decreases in relative humidity over the South Hemisphere (Fischer & Knutti, 2013). It is been suggested that the changes of dry-bulb temperature and relative humidity during extremely hot days are negatively correlated over most areas of the world in both current and future climate (Fischer & Knutti, 2013). Notably the relative changes of Tx (Figure 1(d)) are lower than those of TWx (Figure 1(b)) in most regions of the world, indicating that extreme TWs is more sensitive to the changing climate and the future changes are more detectable than the extreme Ts. Even though the projected changes in TWx and Tx in MME are robust all over the land regions (Figure S5), their magnitudes differ

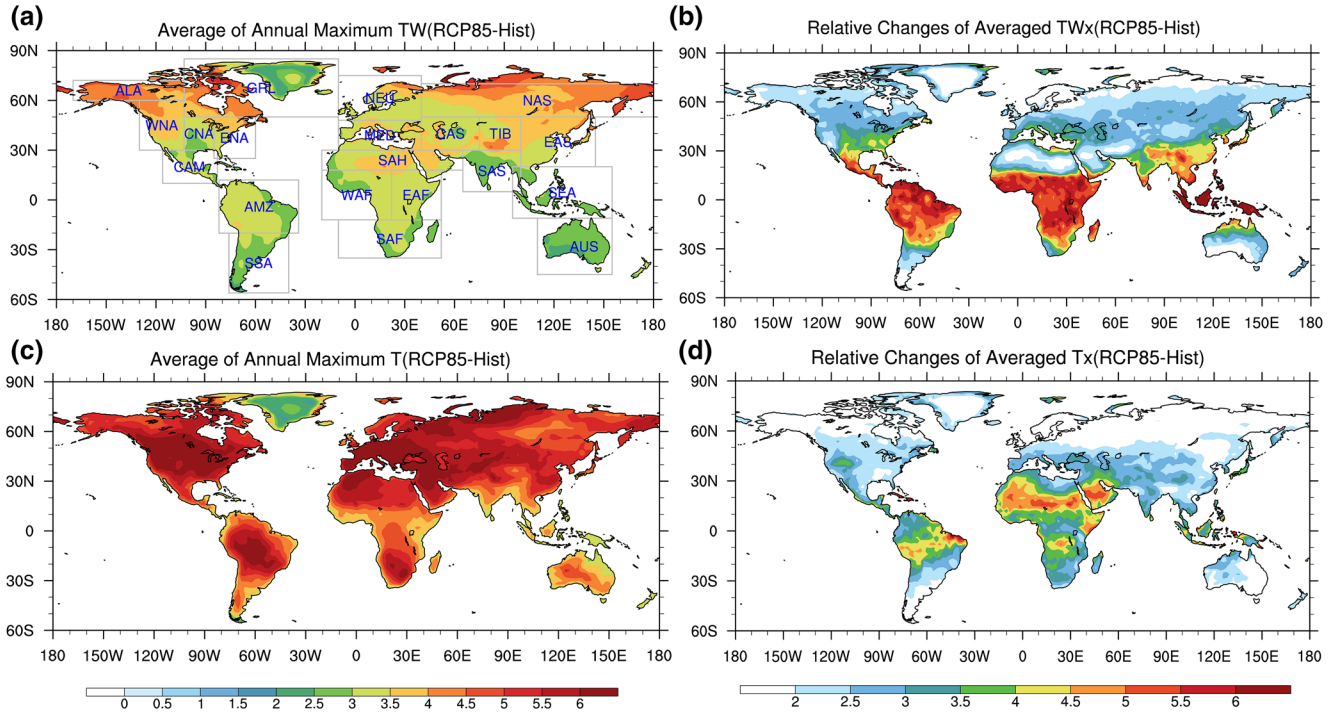

Figure 1. Future changes in the average annual maximum TW and T (TWx and Tx) in the MME between the RCP8.5 and Hist experiments (RCP85-Hist). Absolute changes of average TWx and Tx (a, c; unit: °C). Relative changes of averaged TWx and Tx normalized by the interquartile (IQR) values during the historical period (b, d). The 21 subregions are outlined in Figure 1a: AUS, Australia; AMZ, Amazon Basin; SSA, Southern South America; CAM, Central America; WNA, Western North America; CNA, Central North America; ENA, Eastern North America; ALA, Alaska; GRL, Greenland; MED, Mediterranean Basin; NEU, Northern Europe; WAF, Western Africa; EAF, Eastern Africa; SAF, Southern Africa; SAH, Sahara; SEA, Southeast Asia; EAS, East Asia; SAS, South Asia; CAS, Central Asia; TIB, Tibet; NAS, North Asia. MME, multimodel ensemble mean.

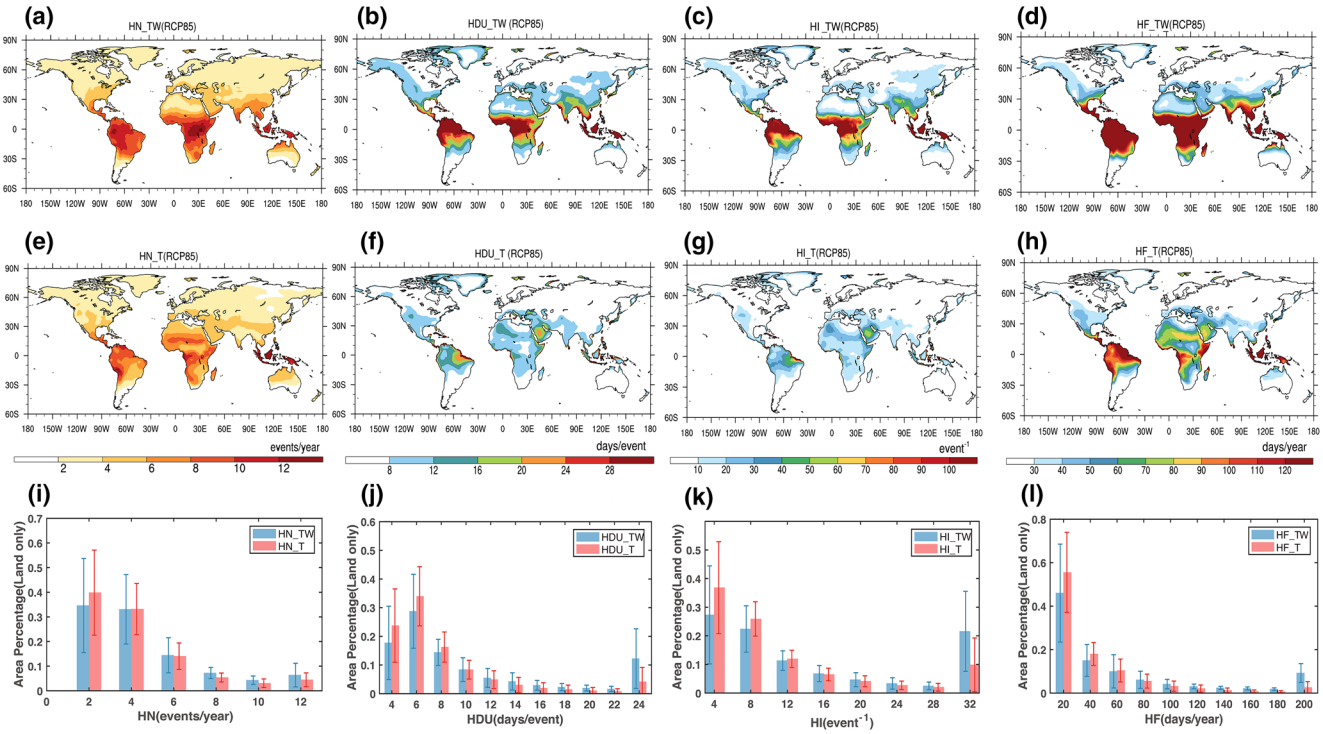

Figure 2. Projected heat indices based on TW and T in the MME under the RCP8.5 scenario. The upper and middle rows show the spatial pattern of mean HN (events/year), HDU (days/event), HI (event^{-1}), and mean HF (days/year) based on TW (a–d) and T (e–h), respectively. The projected heat indices in MME are robust over all the land regions that the intermodel spread is lower than the absolute values of MME. The bottom row (i–l) shows the histograms of area percentages for the four heat indices in the MME under the RCP8.5 scenario. Error bars denote one standard deviation of 18 CMIP5 models. MME, multimodel ensemble mean.

among the 18 GCMs, with relatively higher values in BNU-ESM, CANESM2, GFDL-CM3, IPSL-CM5A-LR, and MIROC-ESM than the others (Figures S6 and S7). Compared to the low-emission scenario (RCP4.5, shown in Figure S8), both the absolute and relative changes of the average TWx and Tx in RCP8.5 scenario show similar spatial pattern but with amplified magnitudes.

3.2. Projected Extreme Heat Events in Future Climate

As both extreme TWs and Ts increase globally, extreme heat events are expected to occur more frequently in the future. The projected humid and dry heat indices based on TW and T under RCP8.5 are shown in Figure 2. For both humid and dry heat events, all four heat event indices (i.e., HN, HDU, HI, and HF) show higher magnitudes over the tropical regions, consistent with previous work (e.g., Matthews, 2018). The humid heat indices are of higher magnitudes than the dry heat indices in most regions. For example, HN_TW are higher than 10 events/year over Amazon Basin, Eastern Africa (AMZ and EAF subregions), but HN_T is generally lower than eight events/year over the same regions (Figures 2(a) and 2(e)). Substantial intensification is also seen for HDU_TW, HI_TW, and HF_TW (Figures 2(b)–2(d)) compared to HDU_T, HI_T, and HF_T (Figures 2(f)–2(h)). The results suggest that when the effects of moisture are included, humid heat events are projected to have longer duration and higher intensity and frequency than dry heat events in the future.

Comparing the percentage of areas with different heat index values shows that more areas experience low occurrences (two events/year) of dry heat events (HN_T) than humid heat events (HN_TW), but at high occurrences of >6 events/year, more areas experience humid heat events than dry heat events (Figure 2(i)). Similar differences are also found between humid and dry heat events for the area percentages of HDU_TW (HI_TW, HF_TW) and HDU_T (HI_T, HF_T) (Figures 2(j), 2(k), and 2(l)). For example, there are significantly more areas with duration >24 days and intensity >32 times the climatological IQR for humid heat

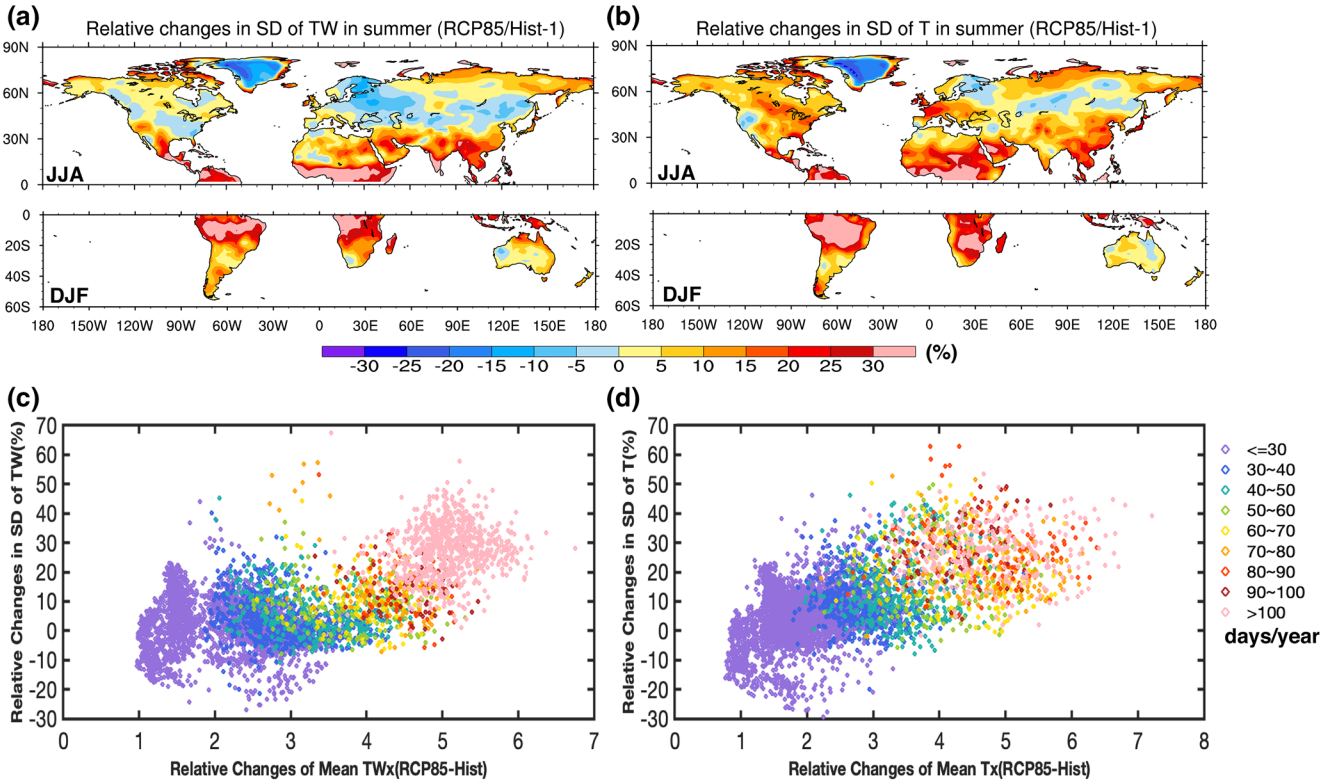

Figure 3. Relative changes in SD of daily TW (a) and T (b) anomalies in summer projected in MME under RCP8.5 scenario. Boreal summer: June, July, and August (JJA); austral summer: December, January, and February (DJF). The lower panel shows the scatterplot of annual mean HF_TW (c) and HF_T (d) coordinated by relative changes in mean TWx and Tx (*x* axis) and relative changes in SD of daily TW of T anomalies (*y* axis) under RCP8.5. Each dot represents a particular land grid cell. SD, standard deviation; MME, multimodel ensemble mean.

events than dry heat events (Figures 2(j) and 2(k)), with the differences residing mostly in the tropics (Figures 2(b), 2(c), 2(f), and 2(g)). Hence, more areas will experience higher frequency, more intense, longer duration, and more total number of days of humid heat events than dry heat events in the future. Moreover, the spatial patterns of the differences between HN_TW (DU_TW, HI_T, HF_TW) and HN_T (HDU_T, HI_T, HF_T) reveal that the intensification of humid heat events relative to dry heat events is more obvious in tropical regions (figure not shown). The intensification of humid heat events is also consistent with the intrinsic and distinct atmospheric environments during humid and dry heat events, represented as different atmospheric moisture content. Extreme Ts is generally convection inhibited with decreased moisture and anomalously descending motions while extreme TWs can be convection favored with increased moisture and ascending motions (Coffel et al., 2018; Wang et al., 2017, 2019). In other words, the increased humidity can favor the occurrences of increased TWs (humid heat events) while the convection accompanied with humid heat can dampen increases of Ts. The differences in atmospheric moisture content during humid and dry heat events are also true in the warmer climate (Figure S9). The projected mean and extreme specific humidity shows notable increases in the future warmer climate, especially over the tropics (Figure S10), which favors the intensified humid heat events therein. Under the RCP4.5 scenario, both humid and dry heat events show spatial patterns comparable to those under RCP8.5, but with lower magnitudes (Figure S11).

Previous studies have strengthened the impacts of variability and mean values in temperatures on heat waves under global warming (e.g., Perkins, 2015). Here, we use the relative changes in standard deviation (SD) of daily TW/T anomalies between historical and future climate to characterize the future changes in the variability of TW/T in a warmer climate. Daily TW/T anomaly value represents the deviation from the 25-year mean of the same date at a particular grid cell in historical (1981–2005) and future (2076–2100). To eliminate the regional impacts of background levels of TW/T variability, we analyze changes in SD in relative terms (Fut/Hist-1). As shown in Figure 3(a) and 3(b), TW and T in summer season show unequal

changes in SD, with decreases outside the tropics but increases over the tropical regions, and relatively higher increases over Amazon Basin (AMZ), Western Africa (WAF), Eastern Africa (EAF), and Southeastern Asia (SEA), consist with previous finding (Bathiany et al., 2018). In fact, changes in SD of daily TW/T through the whole year between Hist and Fut show similar spatial features (figures not shown). The scatterplots in Figures 3(c) and 3(d) show that the changes in HF_TW and HF_T are associated with both the changes in mean values and SD of TW and T. It should be noted that, with relative SD lower than around 10%, the increases of heat events seem to depend only on the increases of the mean values of TW/T (the points locate horizontally) while the increases in relative SD accelerate the increasing rate of heat events (the points are located more vertical) when relative changes in SD are higher. Therefore, the inequal changes in variability of TW and T amplify the impacts of unequal changes in mean values. In other words, the joint impacts of changes in mean value and variability of TW/T are responsible for the unequal increase in heat events to mean global warming. Over the tropical regions, both the mean values and variability of TW/T show higher increases, thus HF_TW/T over tropical regions increase more than the mean warming suggest. It can be concluded that, because of the joint impacts of increases in mean values and variability in TW and T, tropics regions are most vulnerable to projected extreme heat events (both humid and dry) under global warming.

Lastly, we quantify the impacts of different climate warming levels on heat events. Figure 4 show the seasonal cycle of the occurrence of humid and dry heat events based on TW and T projected by the MME under RCP4.5 and RCP8.5 scenarios, respectively. Under RCP4.5, the tropical region as a whole is affected by both humid and dry heat events nearly throughout the year but the midlatitude regions experience heat events mainly in summer (Figures 4(a) and 4(b)). Also, compared to RCP4.5, both the occurrences of humid and dry heat events show apparent increases in RCP8.5 (Figures 4(c) and 4(d)). Notably, both humid and dry heat events occur earlier in the warm season in the midlatitudes and last longer (from June to September in the Northern Hemisphere and from December to March in the Southern Hemisphere) and affect a wider range of latitudes in the tropics in RCP8.5. Such obvious increases in extreme heat events under the high-emission scenario would threaten human health of a larger population. It is worthy to mention that, the monthly occurrences of humid and dry heat events show similar distributions but with shifts in their average occurrence month (Figure S12). And we use the deviation of the average occurrence month between humid and dry heat events to loosely represent their difference in occurrence time. It is found that dry heat events tend to be ahead of humid heat events over nearly all land regions, and such shifts in time are more obvious over tropics (up to 1 month). For instance, over SAS, the mean occurrence time of dry heat events is more than 1 month ahead of humid heat events (Figure S12r).

4. Discussion and Conclusions

In this study, future changes in extreme humid and dry heat events consisting of consecutive days of extreme TWs and Ts projected by 18 CMIP5 GCM simulations are investigated globally and regionally. Projected characteristics of humid and dry heat events including their frequency, duration, and intensity are analyzed. Based on the MME results, humid and dry heat events based on TW and T in the future occur more frequently over the tropical regions, with humid heat events intensifying more relative to dry heat events. Future heat events and the intensification of humid heat events over dry heat events are larger in the tropics because of the joint impacts of changes in mean values and variability of TW and T. Over tropics, both the relative changes in mean values and variability of TW/T are higher. Thus, future heat events (both humid and dry) will emerge more prominently above the noise over tropical regions. Comparison of the projected heat events under the RCP4.5 and RCP8.5 scenarios representing low and high emissions urges more efforts on climate change mitigation and adaptation to address the potential human health effect of extreme heat.

Future changes in atmospheric moisture in the warmer climate are important for the intensification of humid heat events. It is well accepted that dry heat events are dominated by anomalously high-pressure systems, accompanied by the descending motions, reduced moisture, and increased solar radiation (e.g., Della-Marta et al., 2007; Freychet et al., 2017; Wang et al., 2017, 2018). However, the atmospheric conditions associated with extreme TWs are more complicated. A recent study revealed that, during extreme TWs of greater moisture contribution, the large-scale environment favors convection, as indicated by ascending motions, decreased downward solar radiation as well as increased precipitable water and near surface

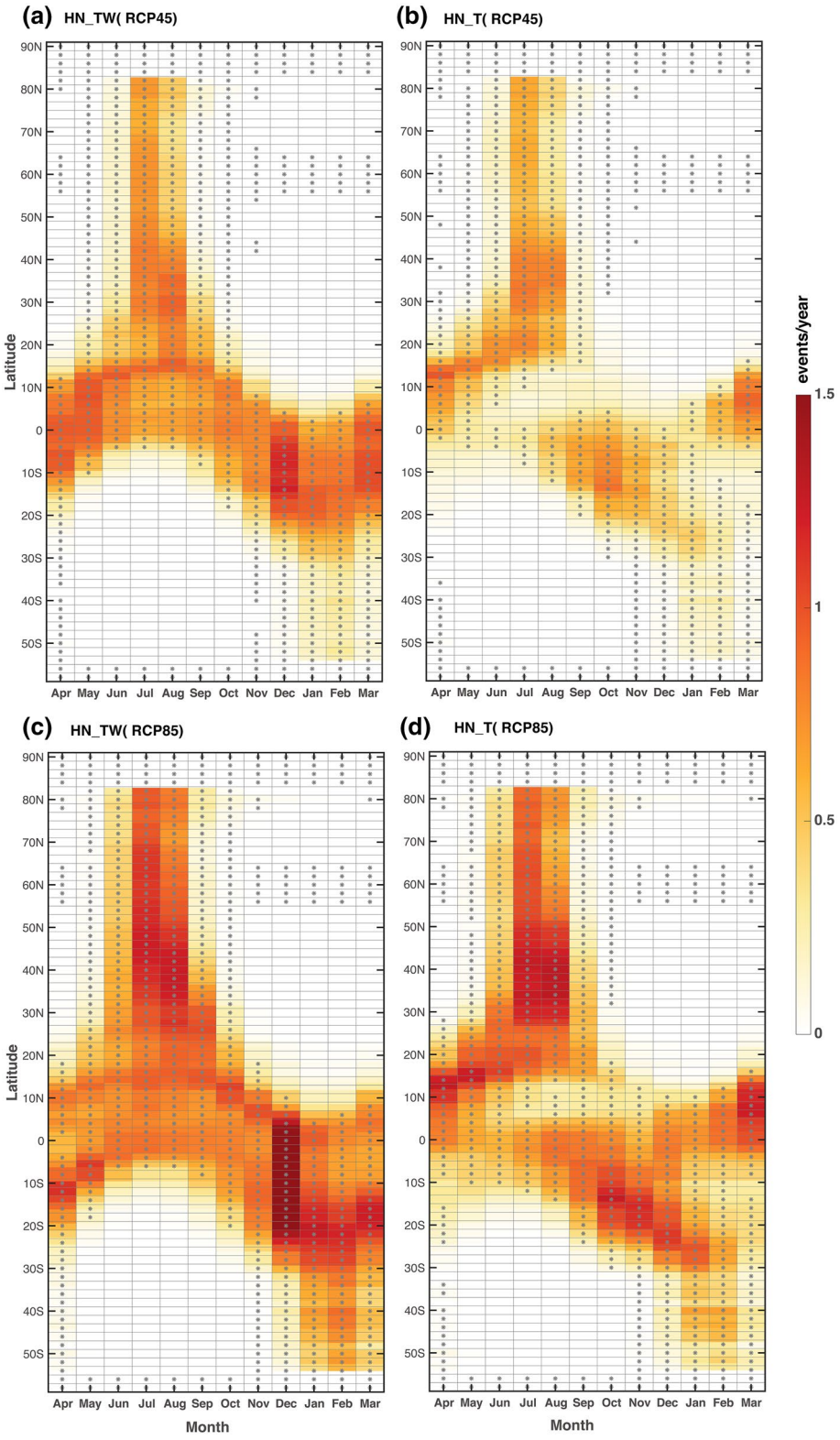

Figure 4. Monthly variations of the projected zonal mean HN_TW and HN_T in the MME under RCP4.5 (the top row) and RCP8.5 (the bottom row). The asterisk indicates the projections in the MME are robust (see caption of Figure S5 for the definition of MME robustness). MME, multimodel ensemble mean.

humidity, while during extreme TWs of greater temperature contribution, the atmospheric conditions are similar to extreme Ts (Wang et al., 2019). Moreover, the projected atmospheric moisture content during humid heat events is notably higher than that during dry heat events in future (Figure S9), supporting the different effects of moisture during humid and dry heat events. Therefore, the enhanced convections associated with increased humidity and heat over the tropics can favor the occurrences of extreme TWs but dampen increases of Ts (Coffel et al., 2018; Wang et al., 2019). In particular, the regional differences in projected specific humidity and temperatures are driven by local dynamic and thermodynamic processes, including the relationship between humid heat and convection over tropics, atmospheric water vapor transport and the influences of anomalous SSTs. Therefore, more works with high-resolution regional climate model are needed to resolve such issues. Understanding the differences among GCMs should be another noteworthy issue. Even though the 18 CMIP5 GCMs show great consistency in simulating the spatial features of extreme TWx/Tx, the differences of annual variations of TWx/Tx among GCMs are apparent (Figures S1(f) and S2(f)). Among the 18 GCMs, BCC-CSM-1-1, BNU-ESM, MIROC5, MRI-CGCM3, and NORESM1-M show relatively lower skills than the others in capturing the annual variability of TWx/Tx. Moreover, the differences of projected regional mean HF_TW/HF_T are also notable among GCMs. ACCESS1-0, ACCESS1-3, CANEMS2, GFDL-CM3, IPSL-CM5A-LR, and MIROC-ESM generally show higher values than the others (Figure S13). The reasons for the differences across different GCMs in simulating extreme TWs/Ts can be related to some key feedbacks such as those involving clouds and the carbon cycle, which deserves further works.

Data Availability Statement

The CMIP5 model results are accessible at https://cerawww.dkrz.de/WDCC/ui/cerasearch/project?acronym=IPCC-AR5_CMIP5

Acknowledgments
This work is supported by the National Key Research and Development Program of China (2016YFA0600303, 2020YFA0607803, and 2019YFA0606800) and the National Natural Science Foundation of China (41975159). L. R. Leung was supported by the U.S. Department of Energy Office of Science Biological and Environmental Research through the Regional and Global Modeling and Analysis program area. The Pacific Northwest National Laboratory (PNNL) is operated for the Department of Energy by Battelle Memorial Institute under contract DE-AC05-76RL01830. The authors acknowledge the World Climate Research Program's Working Group that is responsible for the CMIP and make available their model outputs.

References

Bathiany, S., Dakos, V., Scheffer, M., & Lenton, T. M. (2018). Climate models predict increasing temperature variability in poor countries. *Science Advances*, *4*(5), eaar5809.

Beniston, M., Stephenson, D. B., Christensen, O. B., Ferro, C. A., Frei, C., Goyette, S., et al. (2007). Future extreme events in European climate: An exploration of regional climate model projections. *Climatic Change*, *81*(1), 71–95.

Black, E., Blackburn, M., Harrison, G., Hoskins, B., & Methven, J. (2004). Factors contributing to the summer 2003 European heatwave. *Weather*, *59*(8), 217–223.

Boo, K. O., Kwon, W. T., & Baek, H. J. (2006). Change of extreme events of temperature and precipitation over Korea using regional projection of future climate change. *Geophysical Research Letters*, *33*, L01701. https://doi.org/10.1029/2005GL023378

Budd, G. M. (2008). Wet-bulb globe temperature (WBGT)—Its history and its limitations. *Journal of Science and Medicine in Sport*, *11*(1), 20–32.

Buzan, J. R., Oleson, K., & Huber, M. (2015). Implementation and comparison of a suite of heat stress metrics within the Community Land Model version 4.5. *Geoscientific Model Development*, *8*(2), 151–170. https://doi.org/10.5194/gmd-8-151-2015

Coffel, E. D., Horton, R. M., & de Sherbinin, A. (2018). Temperature and humidity based projections of a rapid rise in global heat stress exposure during the 21st century. *Environmental Research Letters*, *13*(1), 014001. https://doi.org/10.1088/1748-9326/aaa00e

Conti, S., Meli, P., Minelli, G., Solimini, R., Toccaceli, V., Vichi, M., et al. (2005). Epidemiologic study of mortality during the Summer 2003 heat wave in Italy. *Environmental Research*, *98*(3), 390–399. https://doi.org/10.1016/j.envres.2004.10.009

Davies-Jones, R. (2008). An efficient and accurate method for computing the wet-bulb temperature along pseudoadiabats. *Monthly Weather Review*, *136*(7), 2764–2785.

Davis, R. E., McGregor, G. R., & Enfield, K. B. (2016). Humidity: A review and primer on atmospheric moisture and human health. *Environmental Research*, *144*, 106–116.

Dee, D. P., Uppala, S. M., Simmons, A. J., Berrisford, P., Poli, P., Kobayashi, S., et al. (2011). The ERA-Interim reanalysis: Configuration and performance of the data assimilation system. *Quarterly Journal of the Royal Meteorological Society*, *137*(656), 553–597.

Della-Marta, P. M., Luterbacher, J., von Weissenfluh, H., Xoplaki, E., Brunet, M., & Wanner, H. (2007). Summer heat waves over western Europe 1880–2003, their relationship to large-scale forcings and predictability. *Climate Dynamics*, *29*(2–3), 251–275.

Dole, R., Hoerling, M., Perlwitz, J., Eischeid, J., Pegion, P., Zhang, T., et al. (2011). Was there a basis for anticipating the 2010 Russian heat wave? *Geophysical Research Letters*, *38*, L06702. https://doi.org/10.1029/2010GL046582

Dong, L., Leung, L. R., Song, F., & Lu, J. (2018). Roles of SST versus internal atmospheric variability in winter extreme precipitation variability along the U.S. West Coast. *Journal of Climate*, *31*(19), 8039–8058.

Dosio, A., Mentaschi, L., Fischer, E. M., & Wyser, K. (2018). Extreme heat waves under 1.5°C and 2°C global warming. *Environmental Research Letters*, *13*(5), 054006.

Dunn, R. J. H., Willett, K. M., Thorne, P. W., Woolley, E. V., Durre, RI., Dai, A., et al. (2012). HadISD: A quality-controlled global synoptic report database for selected variables at long-term stations from 1973–2011. *Climate of the Past*, *8*, 1649–1679.

Dunn, R. J. H., Willett, K. M., Parker, D. E., & Mitchell, L. (2016). Expanding HadISD: Quality-controlled, sub-daily station data from 1931. *Geoscientific Instrumentation, Methods and Data Systems*, *5*, 473–491.

Fischer, E. M., & Knutti, R. (2013). Robust projections of combined humidity and temperature extremes. *Nature Climate Change*, *3*(2), 126.

Freychet, N., Tett, S., Wang, J., & Hegerl, G. (2017). Summer heat waves over Eastern China: Dynamical processes and trend attribution. *Environmental Research Letters*, *12*(2), 024015. https://doi.org/10.1088/1748-9326/aa5ba3

Giorgi, F., & Francisco, R. (2000). Evaluating uncertainties in the prediction of regional climate change. *Geophysical Research Letters*, *27*(9), 1295–1298. https://doi.org/10.1029/1999GL011016

Caulfield, M. P., Cambridge, H., Foster, S. F., & McGreevy, P. D. (2014). Heat stress: A major contributor to poor animal welfare associated with long-haul live export voyages. *The Veterinary Journal*, *199*(2), 223–228. http://dx.doi.org/10.1016/j.tvjl.2013.09.018

Hanna, E. G., & Tait, P. W. (2015). Limitations to thermoregulation and acclimatization challenge human adaptation to global warming. *International Journal of Environmental Research and Public Health*, *12*(7), 8034–8074.

Huang, H., Hammerling, D., Li, B., & Smith, R. (2019). *Combining interdependent climate model outputs in CMIP5: A spatial Bayesian approach. arXiv preprint arXiv:2001.00074*.

Kanamitsu, M., Ebisuzaki, W., Woollen, J., Yang, S.-K., Hnilo, J., Fiorino, M., & Potter, G. L. (2002). NCEP-DOE AMIP-II reanalysis (R-2). *Bulletin of the American Meteorological Society*, *83*, 1631–1643.

Kang, S., & Eltahir, E. A. (2018). North China Plain threatened by deadly heatwaves due to climate change and irrigation. *Nature Communications*, *9*(1), 2894.

Koutroulis, A. G., Grillakis, M. G., Tsanis, I. K., & Papadimitriou, L. (2016). Evaluation of precipitation and temperature simulation performance of the CMIP3 and CMIP5 historical experiments. *Climate Dynamics*, *47*(5–6), 1881–1898.

Kumar, D., Kodra, E., & Ganguly, A. R. (2014). Regional and seasonal intercomparison of CMIP3 and CMIP5 climate model ensembles for temperature and precipitation. *Climate Dynamics*, *43*(9–10), 2491–2518.

Kunkel, K. E., Liang, X. Z., & Zhu, J. (2010). Regional climate model projections and uncertainties of US summer heat waves. *Journal of Climate*, *23*(16), 4447–4458.

Lenssen, N. J. L., Schmidt, G. A., Hansen, J. E., Menne, M. J., Persin, A., Ruedy, R., & Zyss, D. (2019). Improvements in the GISTEMP uncertainty model. *Journal of Geophysical Research: Atmosphere*, *124*, 6307–6326. https://doi.org/10.1029/2018JD029522

Li, C., Zhang, X., Zwiers, F., Fang, Y., & Michalak, A. M. (2017). Recent very hot summers in northern hemispheric land areas measured by wet bulb globe temperature will Be the norm within 20 years. *Earth's Future*, *5*, 1203–1216. https://doi.org/10.1002/2017EF000639

Matsueda, M. (2011). Predictability of Euro-Russian blocking in summer of 2010. *Geophysical Research Letters*, *38*, L06801. https://doi.org/10.1029/2010GL046557

Matthews, T. (2018). Humid heat and climate change. *Progress in Physical Geography: Earth and Environment*, *42*(3), 391–405.

Mora, C., Counsell, C. W., Bielecki, C. R., & Louis, L. V. (2017). Twenty-seven ways a heat wave can kill you: Deadly heat in the era of climate change. *Circulation: Cardiovascular Quality and Outcomes*, *10*(11), e004233.

Mukherjee, S., Ashfaq, M., & Mishra, A. K. (2020). Compound drought and heatwaves at a global scale: The role of natural climate variability-associated synoptic patterns and land-surface Energy budget anomalies. *Journal of Geophysical Research: Atmosphere*, *125*, e2019JD031943. https://doi.org/10.1029/2019JD031943

Perkins, S. E. (2015). A review on the scientific understanding of heatwaves—Their measurement, driving mechanisms, and changes at the global scale. *Atmospheric Research*, *164*, 242–267.

Raymond, C., Matthews, T., & Horton, R. (2020). The emergence of heat and humidity too severe for human tolerance. *Science Advances*, *6*(19), eaaw1838.

Raymond, C., Singh, D., & Horton, R. (2017). Spatiotemporal patterns and synoptics of extreme wet-bulb temperature in the contiguous United States. *Journal of Geophysical Research: Atmosphere*, *122*, 13108–13124. https://doi.org/10.1002/2017JD027140

Pielke, R. A., Avissar, R., Raupach, M., Dolman, A. J., Zeng, X., & Denning, A. S. (1998). Interactions between the atmosphere and terrestrial ecosystems: influence on weather and climate. *Global Change Biology*, *4*(5), 461–475. https://doi.org/10.1046/j.1365-2486.1998.t01-1-00176.x

Sherwood, S. C., & Huber, M. (2010). An adaptability limit to climate change due to heat stress. *Proceedings of the National Academy of Sciences*, *107*(21), 9552–9555.

Stéfanon, M., Drobinski, P., d'Andrea, F., & de Noblet-Ducoudré, N. (2012). Effects of interactive vegetation phenology on the 2003 summer heat waves. *Journal of Geophysical Research*, *117*, D24103. https://doi.org/10.1029/2012JD018187

Taylor, K. E., Stouffer, R. J., & Meehl, G. A. (2012). An overview of CMIP5 and the experiment design. *Bulletin of the American Meteorological Society*, *93*(4), 485–498.

Trenberth, K. E., Jones, P. D., Ambenje, P., Bojariu, R., Easterling, D., Klein Tank, A., et al (2007). In Observations: surface and atmospheric climate change. Chapter 3. *Climate change*, (pp. 235–336). Cambridge: Cambridge University Press. Retrieved from https://www.ipcc.ch/site/assets/uploads/2018/02/ar4-wg1-chapter3-1.pdf

Wang, P., Leung, L. R., Lu, J., Song, F., & Tang, J. (2019). Extreme wet-bulb temperatures in China: The significant role of moisture. *Journal of Geophysical Research: Atmosphere*, *124*(22) 11944–11960. https://doi.org/10.1029/2019JD031477

Wang, P., Tang, J., Sun, X., Wang, S., Wu, J., Dong, X., & Fang, J. (2017). Heat waves in China: Definitions, leading patterns, and connections to large-scale Atmospheric circulation and SSTs. *Journal of Geophysical Research: Atmosphere*, *122*, 10679–10699. https://doi.org/10.1002/2017JD027180

Wang, P., Tang, J., Wang, S., Dong, X., & Fang, J. (2018). Regional heatwaves in China: A cluster analysis. *Climate Dynamics*, *50*(5–6), 1901–1917. https://doi.org/10.1007/s00382-017-3728-4

Willet, K. M., & Sherwood, S. C. (2012). Exceedance of heat index thresholds for 15 regions under a warming climate using the wet-bulb globe temperature. *International Journal of Climatology*, *32*, 161–177. https://doi.org/10.1002/jocjoc.2257

Xia, J., Tu, K., Yan, Z., & Qi, Y. (2016). The super-heat wave in eastern China during July–August 2013: A perspective of climate change. *International Journal of Climatology*, *36*(3), 1291–1298.

Zhao, T., Chen, L., & Ma, Z. (2014). Simulation of historical and projected climate change in arid and semiarid areas by CMIP5 models. *Chinese Science Bulletin*, *59*(4), 412–429. https://doi.org/10.1007/s11434-013-0003-x

Zhai, P., Zhou, B., & Chen, Y. (2018). A Review of Climate Change Attribution Studies. *Journal of Meteorological Research*, *32*(5), 671–692. https://doi.org/10.1007/s13351-018-8041-6